RSC Advances

PAPER

Cite this: *RSC Adv.*, 2019, **9**, 3605

Designing indacenodithiophene based non-fullerene acceptors with a donor–acceptor combined bridge for organic solar cells†

Muhammad Ans,[a] Khurshid Ayub,[b] Ijaz Ahmad Bhatti[a] and Javed Iqbal *[ac]

Non-fullerene small acceptor molecules have gained significant attention for application in organic solar cells owing to their advantages over fullerene based acceptors. Efforts are continuously being made to design novel acceptors with greater efficiencies. Here, optoelectronic properties of four novel acceptor–donor–acceptor (A–D–A) type small molecules (**A1**, **A2**, **A3** and **A4**) were studied for their applications in organic solar cells. These molecules contain an indacenodithiophene central core unit joined to different end capped acceptors through a monofluoro substituted benzothiadiazole (FBT) donor acceptor (DA) bridge. The different end capped acceptor groups are; 2-2(2-ethylidene-5,6-difluoro-3-oxo-2,3-dihydroinden-1-ylidene)malononitrile (**A1**), 2-2(2-ethylidene-3-oxo-2,3-dihydroinden-1-ylidene)malononitrile (**A2**), 2-(5-ethylidene-6-oxo-5,6-dihydrocyclopenta-*b*-thiophene-4-ylidene)malononitrile (**A3**), and 2-2(2-ethylidene-5,6-dicyano-3-oxo-2,3-dihydroinden-1-ylidene)malononitrile (**A4**). The calculated optoelectronic properties of the designed molecules were compared with a well-known reference compound **R**, which was recently synthesized and reported as being an excellent A–D–A type acceptor molecule. All designed molecules showed the appropriate frontier molecular orbital diagram for a charge transfer. **A4** shows the highest absorption maximum (λ_{max}) of 858.6 nm (in chloroform solvent), which was attributed to the strong electron withdrawing end-capped acceptor group. Among all of the designed molecules, **A3** exhibits the highest open circuit voltages (V_{oc}) which was (1.84 V) with **PTB7-Th** and (1.76 V) with the P3HT donor polymer. Owing to a lower value of λ_e with respect to λ_h, the designed molecules demonstrated superior electron mobilities when compared with reference **R**. Among all of the molecules, **A4** shows the highest electron mobility owing to the lower value of λ_e compared to **R**.

Received 10th November 2018
Accepted 5th January 2019

DOI: 10.1039/c8ra09292c

rsc.li/rsc-advances

1. Introduction

One of the major problems faced today across the globe is an energy crisis. Non-renewable energy sources have been used since ancient times. These energy sources are not only vanishing quickly but also have adverse effects on the environment upon combustion. Many alternative sources such as wind power, hydro power, biomass, and solar cells have gained significant attention in energy conversion devices. Among these, solar cells are quite important owing to the abundance of sunlight available. Solar cells convert sunlight directly into electricity by the photoelectric effect. In the past, silicon was widely used as a semiconducting material in solar cells owing to the high thermal stability, large natural abundance, reduced toxicity and high power conversion efficiency (PCE). However, there are some limitations associated with silicon such as the high cost, hardness and non-tunable energy levels. Recently, organic solar cells have emerged as a low cost alternative to silicon based solar cells. The organic solar cells offer tunable energy levels, solution processability, transparency, a large area of fabrication and flexibility.[1–5] In bulk heterojunction (BHJ) organic solar cells, power conversion efficiencies (PCEs) of 11–12% have been achieved using fullerene acceptor based ($PC_{61}BM$ and $PC_{71}BM$) solar cells.[6–9] Fullerene derivatives have excellent properties such as a high electron mobility, isotropic charge transfer, low reorganization energy and so forth.[10,11] Despite these advantages, the use of fullerenes in solar cells is limited owing to several factors, such as difficulty in tuning the energy level, weak absorption in the visible region, instability, poor solubility, and high production cost.[12–16] To overcome the limitations of fullerene, researchers are focusing on designing solar cells based on non-fullerene acceptors. Non-fullerene electron acceptors have many advantages such as good solubility, strong absorption in the visible region, and tunable energy levels.[17–19] Recently, two important classes of non-

[a]*Department of Chemistry, University of Agriculture Faisalabad, 38000, Faisalabad, Pakistan. E-mail: ansbhatti24@gmail.com; javedkhattak79@gmail.com; Javed.iqbal@uaf.edu.pk*

[b]*Department of Chemistry, COMSAT University, Abbottabad Campus, Abbottabad, KPK, 22060, Pakistan*

[c]*Punjab Bio-energy Institute, University of Agriculture, Faisalabad, 38040, Pakistan*

† Electronic supplementary information (ESI) available. See DOI: 10.1039/c8ra09292c

fullerene acceptors have been studied such as the perylene diimide (PDI)[20–22] based acceptor and fused ring electron acceptors (FREAs).[23–41] Many three dimensional (3D) and helical shaped acceptors based on PDI have been reported to have PCEs up to 9% in organic solar cells.[20–22] FREAs such as ITIC contain a indacenodithienothiophene fused core ring, and 2-(3-oxo-2,3-dihydroinden-1-ylidene)malononitrile (INCN) as an end capped acceptor unit. ITIC has gained significant attention owing to its strong absorption in the visible region, high charge mobility, easy purification process and tunable energy levels. At present, a PCE of over 13% can be obtained with FREAs, much higher than the PCEs obtained using a fullerene based acceptor.[35,36]

The benzothiadiazole (BT) unit is also used to design novel small molecules acceptors (SMAs) to obtain a high PCE. BT unit based molecules show a high LUMO (lowest unoccupied molecular orbital) value. In different acceptors, the BT unit is used as a π-bridge between the electron donor (D) and the terminal end capped acceptor group with a linear structure. McCulloch and co-workers first synthesized BT based SMAs (A1–A2–D–A2–A1) namely FBR, in which fluorene was chosen as the electron donor group.[12] This acceptor, when combined with the well-known donor polymer P3HT, exhibits a PCE of 4.11%.[42] Several derivatives of FBR have also been reported for use in organic solar cells, such as replacing the fluorene donor with a fused heterocyclic indacenodithiophene with a different alkyl phenyl side chain (IDT-2BR),[37] 3D spirobifluorene,[39] or angular-shaped dithienonaphthalene (DTNR).[43]

Herein, we have designed four novel acceptor–donor–acceptor (A–D–A) type molecules, namely (**A1**, **A2**, **A3**, and **A4**) which have an indacenodithiophene central core unit joined to different end capped acceptors through a monofluoro substituted benzothiadiazole (FBT) donor acceptor (DA) bridge. The optoelectronic properties of the designed molecules were evaluated with respect to the reference molecule **R**,[44] which was recently reported.

2. Computational details

All calculations were performed using the Gaussian 09 program[45] and the results were visualized through the Gauss-View 5.0 program.[46] The time dependent density functional theory (TD-DFT) calculations were performed for the reference compound **R** with five functionals (ωB97XD,[47] CAM-B3LYP,[48] B3LYP,[49] M06-2X,[50] and MPW1PW91 (ref. 51)) at a 6-31G(d,p) basis set in order to simulate the absorption spectrum. For the validation of the theoretical method, the maximum absorption (λ_{max}) of reference compound **R** was compared with the experimental data. Functional MPW1PW91 with the 6-31G(d,p) level of theory shows the best agreement with the experimental value, therefore this functional was used for further calculations.

The λ_{max} of all molecules were calculated in the gas and solvent phase. The integral equation formalism polarizable continuum model (IEFPCM)[52] model was used to account for the solvent effect. Origin 6.0 program was used for the spectra plotting.[53] The charge transfer, reorganization energies, frontier orbitals and density of states (DOS) calculations were performed at the MPW1PW91/6-31G(d,p) level of theory. Mulliken charges for all of the designed molecules were also performed using the same selected functional and are summarized in the ESI.† Furthermore, the reorganization energies of all of the designed molecules (**A1** to **A4**) including reference **R** were estimated at the MPW1PW91/6-31G(d,p) level of theory. The reorganization energy was divided into two major parts: internal reorganization energy ($\lambda_{int.}$) and external reorganization energy ($\lambda_{ext.}$). The external reorganization deals with the external environmental relaxation, whereas the internal reorganization energy deals with quick changes in the internal structure.

Here, we neglected the external environmental effect in our study and discuss only the internal reorganization energy. Hence, the reorganization energy of the electron (λ_e) and hole (λ_h) are calculated by using the following equations.

$$\lambda_e = [E_0^- - E^-] + [E_-^0 - E_0] \quad (1)$$

$$\lambda_h = [E_0^+ - E_+] + [E_+^0 - E_0] \quad (2)$$

E_-^0 and E_+^0 are the energies of the neutral molecule *via* the optimized geometries of the cation and anion. E_+, E_- are the energies of the cation and anion *via* optimization of the cation and anion of the neutral molecules, and E_0^+, E_0^- are the single point energies of cation and anion after simple optimization of the neutral molecule. E_0 is the single point energy of the neutral molecule at the ground state.

3. Results and discussion

In the current study, different functionals including (MPW1PW91, ωB97XD, CAM-B3LYP, M06-2, and B3LYP) at a 6-31G(d,p) basis set were used for the estimation of the optoelectronic properties of the reference compound **R**. The maximum absorption (λ_{max}) values for compound **R** with MPW1PW91, ωB97XD, CAM-B3LYP, B3LYP, and M06-2X, functionals at the 6-31G(d,p) basis set are 714.27, 530.13, 536.04, 775.45, and 532.72 nm, respectively, while the reported experimental value is 740 nm (Fig. 1).

It is quite obvious that the MPW1PW91/6-31G(d,p) level of theory shows best agreement with the experiments and provides justification for its use in further calculation.

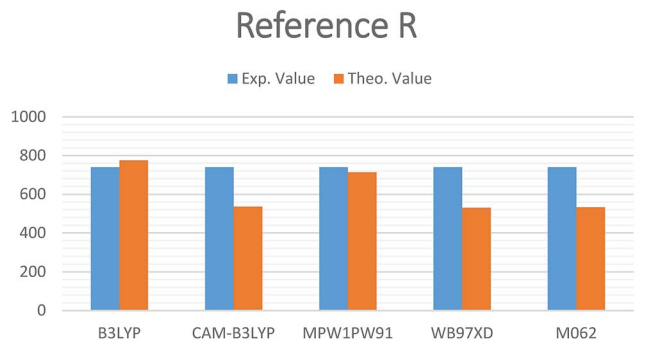

Fig. 1 Simulated bar chart for reference **R** with the B3LYP, CAM-B3LYP, MPW1PW91, ωB97XD and M06-2X at 6-31G(d,p) level of theory.

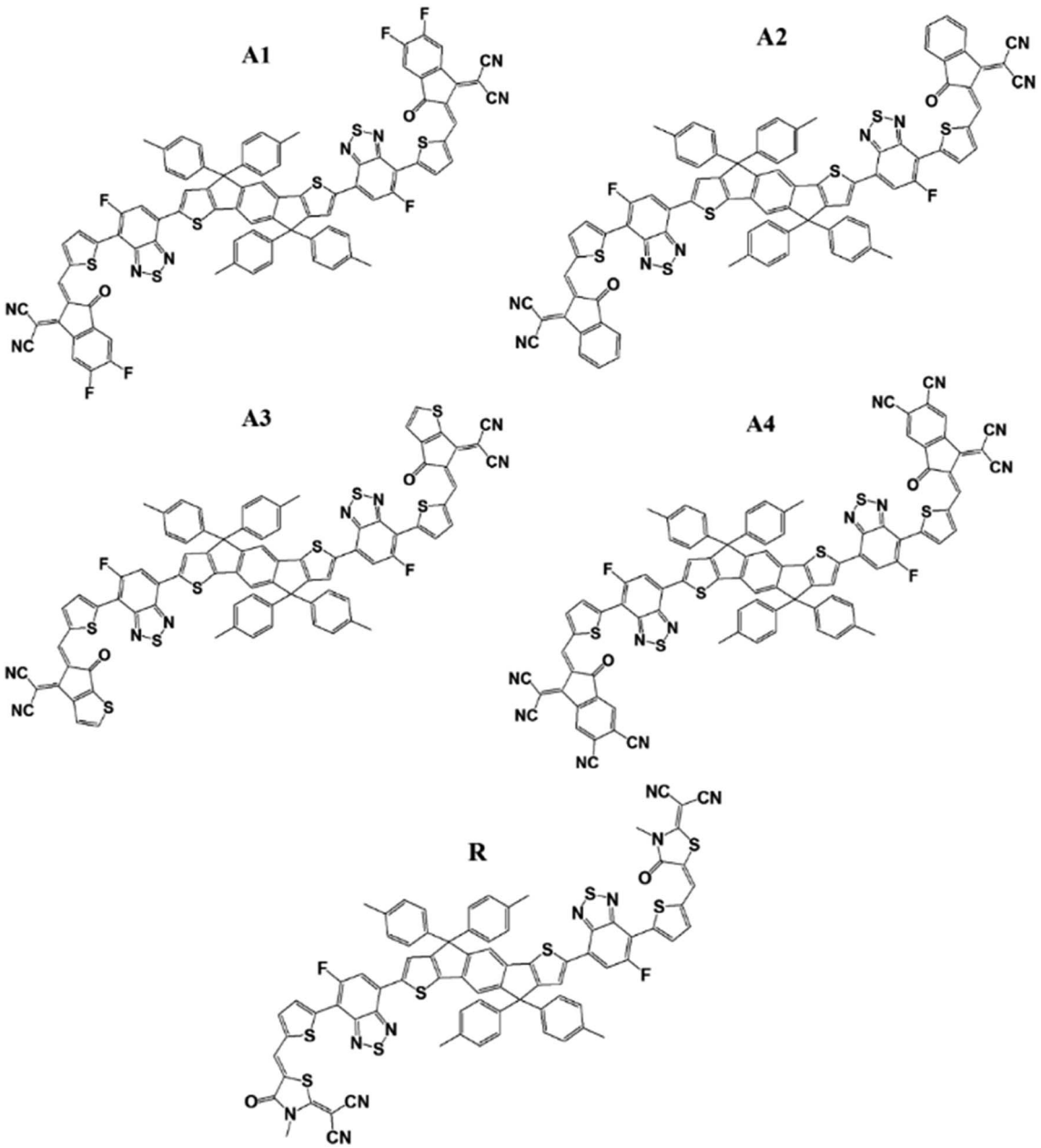

Fig. 2 Molecular structures of reference R and the designed molecules of A1, A2, A3, and A4.

3.1. Frontier molecular orbital diagram

The molecular structures of the reference **R** and designed molecules (**A1**, **A2**, **A3** and **A4**) are shown in Fig. 2.

The optimized geometries of reference **R** and the designed molecules (**A1**, **A2**, **A3**, and **A4**) at the MPW1PW91/6-31G(d,p) level of theory are shown in Fig. 3. The calculated Mulliken charges of all of the molecules are shown in the ESI Fig. S1.† The acceptor, bridge and donor exist in one plane in the optimized geometry while branches on the donor are perpendicular to the plane.

Frontier molecular orbital (FMO) diagrams are a key point used to discuss the opto-electronic properties of Organic Solar Cells (OSCs). The FMO diagrams of all molecules at the MPW1PW91/6-31G(d,p) level of theory are illustrated in Fig. 4. FMO diagrams illustrate the distribution pattern of the electron density in the highest occupied molecular orbital (HOMO) and LUMO. The HOMO and LUMO orbitals energies of the reference compound **R** at MPW1PW91/6-31G(d,p) are −5.49 and −3.35 eV.

The HOMO energies of the designed molecules (**A1**, **A2**, **A3** and **A4**) are −5.57 eV, −5.49 eV, −5.48 eV, and −5.82 eV, respectively, while the LUMO energies are −3.52 eV, −3.41 eV, −3.36 eV and −3.90 eV respectively. The HOMO–LUMO energy gaps of all of the molecules, **A1**, **A2**, **A3** and **A4**, are 2.14 eV, 2.05 eV, 2.08 eV, 2.12 eV, and 1.92 eV respectively. The HOMO and LUMO energies along with their energy gaps are shown in Table 1.

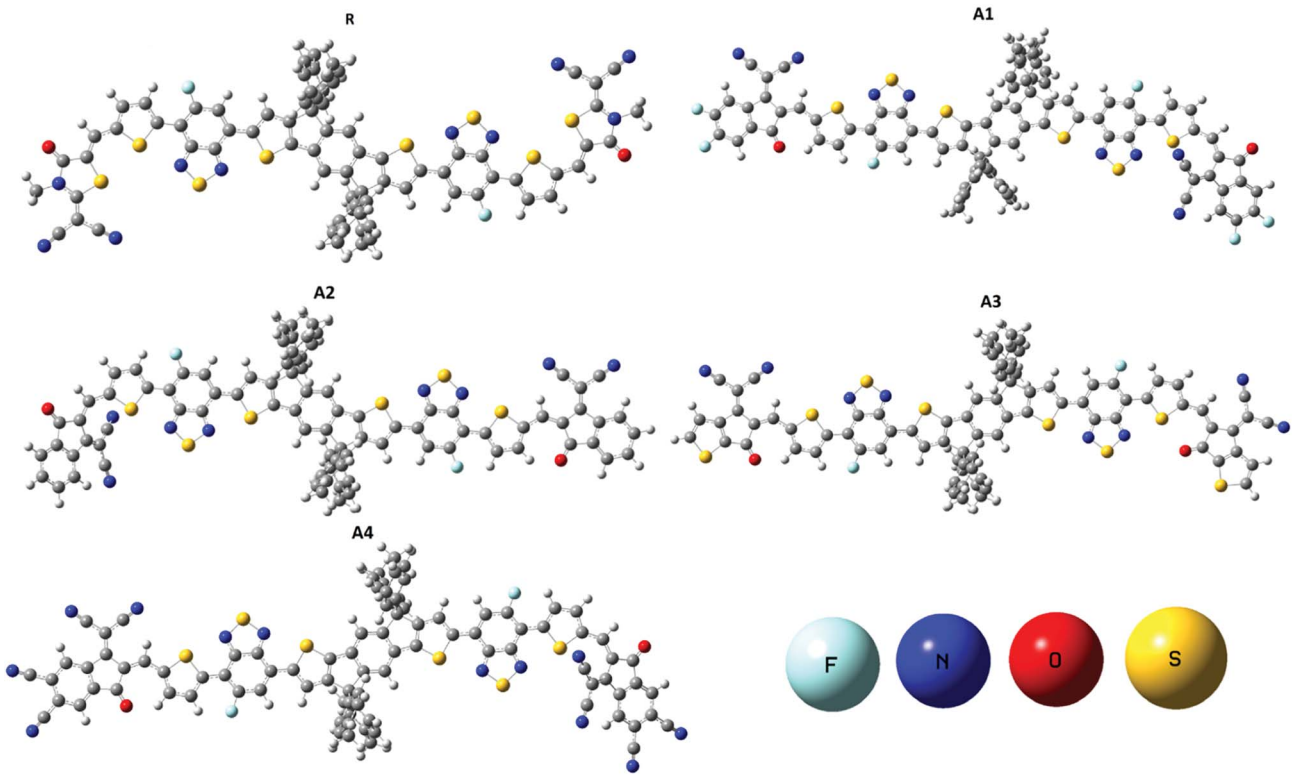

Fig. 3 Optimized geometries of reference R and designed molecules (A1, A2, A3 and A4) at the MPW1PW91/6-31G(d,p) level of theory.

A4 has the lowest HOMO and LUMO values among all of the designed molecules (**A1**, **A2**, and **A3**) including reference **R**, which is attributed to the extended conjugation in the 2-2(2-ethylidene-5,6-dicyano-3-oxo-2,3-dihydroinden-1-ylidene) malononitrile end-capped acceptor group. In the case of **A1**, the HOMO and LUMO values are lower than **A2** and **A3** owing to the fluoro substitution in the end capped group 2-2(2-ethylidene-5,6-difluoro-3-oxo-2,3-dihydroinden-1-ylidene)malononitrile. The HOMO and LUMO energies of **A1** are higher than **A4** because the cyano group has a greater withdrawing effect with respect to fluorine.

The energy of HOMO of **A2** is equal to that of the reference **R**, but the LUMO of **A2** is more stabilized which results in a lower HOMO–LUMO gap in **A2**. Finally, **A3** and **A2** have a comparable HOMO energy level while **A2** has a more stabilized LUMO value mainly due to electron withdrawing effect of 2-2(2-ethylidene-3-oxo-2,3-dihydroinden-1-ylidene)malononitrile in **A2**. The order of the HOMO values for all of the molecules are **A3** > **R** = **A2** > **A1** > **A4**, while the order of the LUMO energies are **R** > **A3** > **A2** > **A1** > **A4**.

The energy gap (E_g) is very important factor for charge transfer. The lower the energy gap, the higher the charge transfer rate. In our study, all of the designed molecules have a lower energy gap with respect to reference **R**. Hence, our designed molecules have better opto-electronic properties than **R**. The energy gaps of all of the molecules are in range of 1.92 to 2.14 eV. The E_g value of reference compound **R** is 2.14 eV. The energy gaps of the designed molecules **A1**, **A2**, **A3**, and **A4** are 2.05, 2.08, 2.12, and 1.92 eV, respectively. Among all of the designed molecules, **A4** (1.92 eV) has the lowest energy gap value owing to the extended conjugation combined with the electron withdrawing end-capped acceptor moiety. **A1** has a higher energy gap value with respect to **A4** owing to the reduced electron withdrawing effect of 2-2(2-ethylidene-5,6-difluoro-3-oxo-2,3-dihydroinden-1-ylidene) malononitrile compared to 2-2(2-ethylidene-5,6-dicyano-3-oxo-2,3-dihydroinden-1-ylidene)malononitrile. Similarly, **A2** has a higher energy gap than **A1** and **A4** but it is lower than **R** owing to the weak effect of 2-2(2-ethylidene-3-oxo-2,3-dihydroinden-1-ylidene)malononitrile. Finally, **A3** has a higher energy gap with respect to (**A1**, **A2** and **A4**) owing to a reduced extended conjugation between the end-capped acceptor groups. The energy gap decreases in the order **A4** < **A1** < **A2** < **A3** < **R**. The HOMO–LUMO values and their energy gaps are expressed in Fig. 5.

To further support the FMO diagram (Fig. 4), a partial density of states (PDOS) analysis of the designed molecules (**A1**–**A4**) and reference **R** at the MPW1PW91/6-31G(d,p) level of theory was performed. DOS spectra of all of the molecules are shown in Fig. 6. It is clearly seen that the electron withdrawing effect of the end-capped acceptor group changes the distribution pattern around the HOMO and LUMO. The HOMO electron density of reference compound **R** is mainly spread on the donor part and donor–acceptor bridge, while the LUMO density is spread uniformly on the entire molecule with a little bit on the acceptor group. In the case of **A1**, the HOMO density is spread mainly on the donor as well as on the bridge group while the lowest unoccupied molecular orbitals (LUMOs) are distributed equally on the donor, acceptor part and little bit on the end-capped acceptor group. The distribution pattern of **A2**

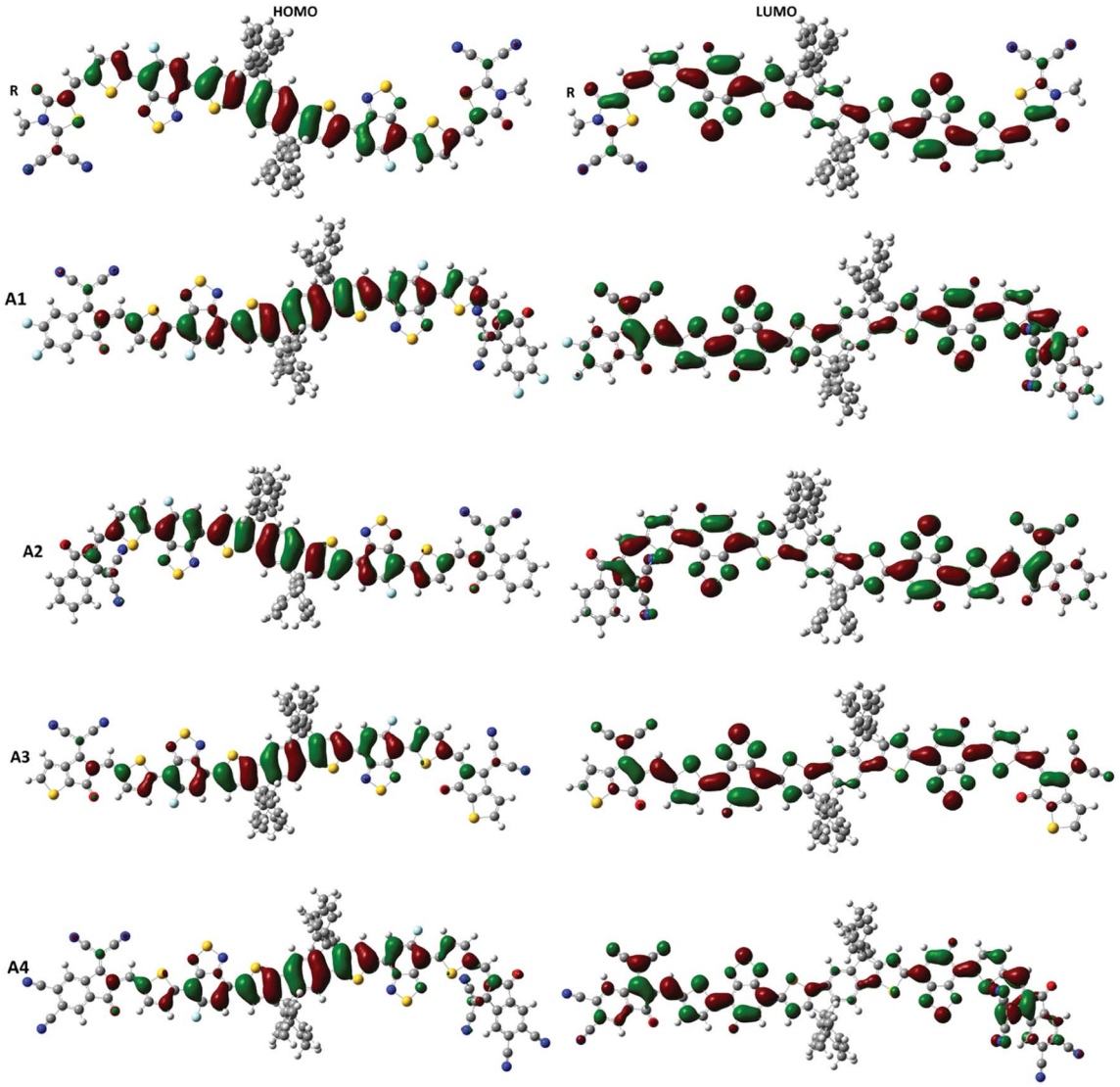

Fig. 4 FMO diagrams of **A1**, **A2**, **A3**, **A4** and reference **R** at the MPW1PW91/6-31G(d,p) level of theory.

resembles, to some extent, **A1**, the highest occupied molecular orbitals (HOMOs) are mainly spread on the donor and bridge unit, while the LUMOs are spread on the donor, bridge unit, and a bit on the end-capped acceptor group. The HOMOs of all of the molecules are mainly on the donor while the LUMOs are mainly on the bridge as well as on the end capped acceptor groups.

Table 1 Energy of HOMO, LUMO and their HOMO–LUMO gap by using the MPW1PW91/6-31G(d,p) level of theory[a]

Molecules	E_{HOMO} (eV)	E_{LUMO} (eV)	E_g (eV)
R	−5.49	−3.35	2.14
A1	−5.57	−3.52	2.05
A2	−5.49	−3.41	2.08
A3	−5.48	−3.36	2.12
A4	−5.82	−3.90	1.92

[a] E_g = Energy band gap.

The distribution pattern for the HOMOs of **A3** and **A4** are quite similar. Both have electron densities on the donor as well as on the bridge unit without an end-capped acceptor moiety, but the pattern of density distribution in the LUMOs is quite different, **A4** has a greater LUMOs distribution on the end-capped acceptor group while **A3** has only a little bit.

4. Optical properties

The UV/Visible absorption spectra were computed at the MPW1PW91/6-31G(d,p) level of theory in the gas phase and in solvent (chloroform) to illustrate the optical properties of the designed molecule (**A1–A4**), see Tables 2 and 3. The maximum absorption λ_{max}, oscillator strength (f), excitation energy, dipole moment and assignment, in the gaseous phase are shown in Table 2.

The results show that the strong electron withdrawing end capped groups with a more extended conjugation cause

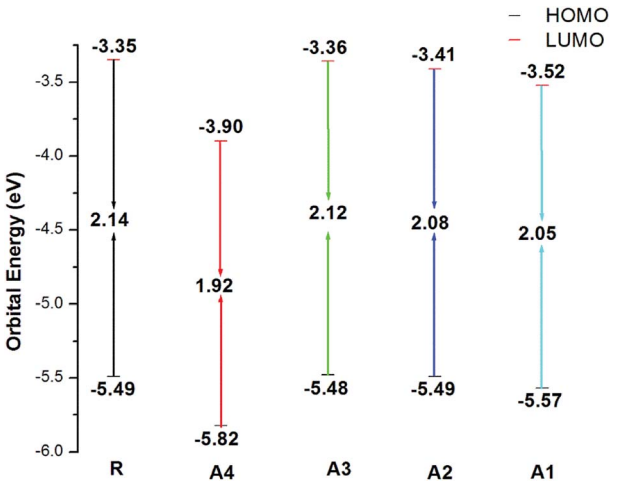

Fig. 5 HOMO–LUMO values of the designed molecules A1, A2, A3, A4 and the reference molecule R at the MPW1PW91/6-31G(d,p) level of theory.

a greater red shift in the absorption spectra.[54] The UV/Visible absorption of all of the molecules lie in the range of 714.3–789.8 nm. The λ_{max} value of the reference compound **R** is 714.3 nm. The compounds **A1–A4** have a higher red shift along with a higher oscillator strength as compared to reference **R**. The λ_{max} values of **A1**, **A2**, **A3**, and **A4** in the gas phase are shown in Table 2. Among all of the molecules, **A4** exhibits a higher red shift and a lower energy gap owing to the extended conjugation of the 2-2(2-ethylidene-5,6-dicyano-3-oxo-2,3-dihydroinden-1-ylidene)malononitrile withdrawing end-capped acceptor moiety.

The λ_{max} value of **A1** is higher than that of **R**, **A2** and **A3** owing to the four fluoro groups which are attached to the end-capped acceptor groups. The λ_{max} values of the designed molecules **A1**, **A2**, **A3** and **A4** are 31.2, 21.8, 6.1, and 75.5 nm, respectively, these are red shifted compared to the reference compound **R** in the gas phase. The order of compounds with respect to the increasing λ_{max} values are **R** < **A3** < **A2** < **A1** < **A4** which is, as expected, the same as the order of the decreasing HOMO–LUMO band gap energy for the compounds. These results suggest that the λ_{max} corresponds to the transition from the HOMO to LUMO which is consistent with the assignment given in Table 2. The simulated absorption spectra of **A1–A4** and **R** are shown in Fig. 7. All of the novel designed molecules have lower exciton energies than that of the reference **R**, which reveals that excitation between HOMO to LUMO is easy. **A4** contains a strong electron withdrawing end capped acceptor group which causes the lower excitation energy and a higher charge transport ability. The order of the excitation energy is **R** < **A3** < **A2** < **A1** < **A4**. The same pattern is observed in the oscillator strength.

The λ_{max} values of reference **R** and the designed molecules (**A1–A4**) in chloroform solvent using the IEFPCM were calculated (see Table 3). The λ_{max} values in solution lie in the range of 742.8–858.6 nm.

The excitation energy from the HOMO to LUMO of all of the designed molecules are in the range of 1.67–1.44 eV. All newly designed molecules have lower excitation energies than the reference **R**, which reveals that excitation between HOMO to LUMO is easy. Lower exciton energy means higher charger transfer, which lead to high power conversion efficiency. Among all, four cyano group with end capped acceptor group in **A4** enhance the absorption maximum. The order of excitation energy is **R** < **A3** < **A2** < **A1** < **A4**, which is similar to absorption pattern. Same pattern observed in oscillator strength. On the basis of above discussion, all newly designed molecules have better absorption, excitation, and oscillator strength than that of reference **R**.

The λ_{max} values in solvent show a similar pattern to that in the gas phase. The absorption maxima for reference compound **R** and the designed molecules **A1**, **A2**, **A3** and **A4** in chloroform are 742.8, 797.2, 784.6, 776.9 and 858.6 nm respectively. Hence, the absorption at the longest wavelength (858.6 nm) was found for **A4** with strong oscillator strength. The red shifts from the vacuum to the chloroform solution for **A1**, **A2**, **A3** and **A4** are 54.4, 41.8, 34.1 and 115.8 nm, respectively. The simulated absorption spectra of **A1–A4** and **R** in chloroform are shown in Fig. 8.

On the basis of the discussion above, all of the designed molecules have better optical properties than reference **R**. All four of the designed molecules have higher λ_{max} values as compared to **R** and may therefore be superior to the reference molecule for use as non-fullerene SMAs.

5. Reorganization energy

Another tool to evaluate the performance of organic solar cells is reorganization energy (electron and hole), reorganization energy is linked with the charge mobilities. Reorganization energy and charge mobilities are in an inverse relationship; the lower the reorganization energy, the higher the charge mobilities. It depends on many factors, but is mainly influenced by the geometry of the cations and anions according to eqn (1) and (2). The anionic geometry indicates the electron transfer from the donor material, while the cationic geometry shows the hole in acceptor material. The overall reorganization can be used to calculate the charger transfer between the donor and acceptor unit. Reorganization is classified into two parts; internal reorganization energy ($\lambda_{int.}$) and external reorganization energy ($\lambda_{ext.}$). The external reorganization deals with the polarization effect on the external environmental while the internal reorganization provides information on quick changes in the internal geometry. Here, we neglect the external environmental effects in our study and discuss only the internal reorganization energy. The reorganization energy of reference **R** including the designed molecules (**A1–A4**) were computed at the MPW1PW91/6-31G(d,p) level of theory. The calculated reorganization energies are expressed in Table 4.

The λ_e value of reference compound **R** is 0.0064 eV. All of the novel designed molecules have a high electron mobility as compared to reference **R**, owing to the low reorganization energy value. Among the molecules, **A4** has the lowest λ_e value, which means that **A4** has the highest electron mobility between the donor and acceptor part. **A1** and **A2** have equal

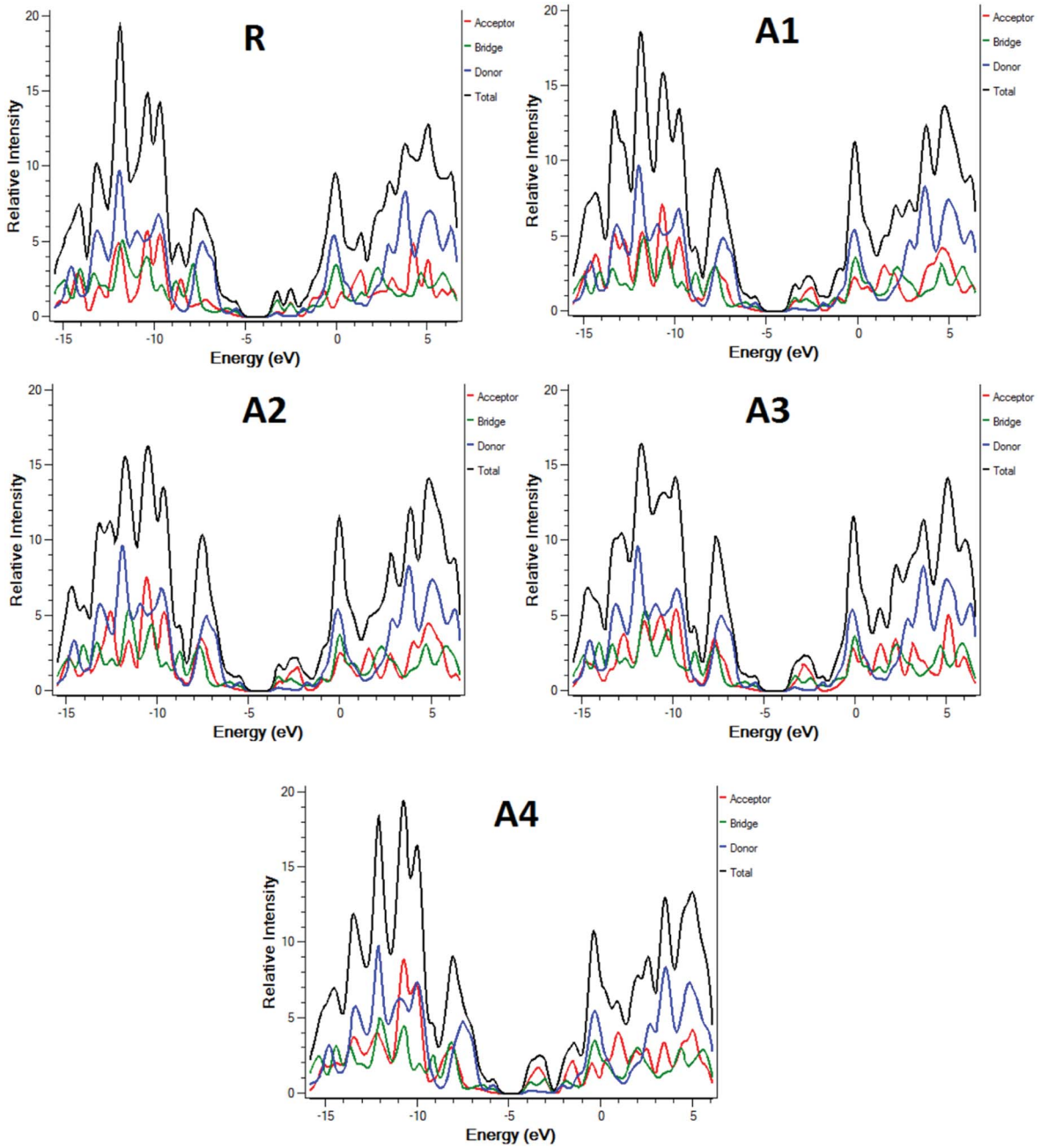

Fig. 6 DOS around the HOMOs and LUMO of reference **R** and the designed molecules **A1**, **A2**, **A3**, **A4** at the MPW1PW91/6-31G(d,p) level of theory.

Table 2 The maximum absorption λ_{max}, oscillator strength (f), excitation energy, dipole moment and assignment, in the gaseous phase at the MPW1PW91/6-31G(d,p) level of theory

Molecules	Calculated λ_{max} (nm)	Exp. λ_{max} (nm)	E_x (eV)	f (oscillator strength)	Assignment	Dipole moment (D)
R	714.3	740 (ref. 44)	1.74	2.73	H > L (+95%)	0.063
A1	745.5	—	1.66	2.99	H > L (+94%)	4.725
A2	736.1	—	1.68	2.98	H > L (+94%)	5.885
A3	720.4	—	1.72	3.17	H > L (+95%)	6.701
A4	789.8	—	1.57	3.03	H > L (+94%)	9.282

Table 3 The maximum absorption λ_{max}, oscillator strength (*f*), excitation energy, dipole moment and assignment, in chloroform solvent at MPW1PW91/6-31G(d,p) level of theory

Molecules	Calculated λ_{max} (nm)	Expected λ_{max} (nm)	E_x (eV)	*f* (Oscillator strength)	Assignment	Dipole moment (*D*)
R	742.8	740 (ref. 44)	1.67	3.01	H > L (+94%)	0.176
A1	797.2	—	1.56	3.20	H > L (+93%)	5.716
A2	784.6	—	1.58	3.23	H > L (+93%)	6.740
A3	776.9	—	1.60	3.57	H > L (+92%)	8.489
A4	858.6	—	1.44	3.24	H > L (+92%)	11.17

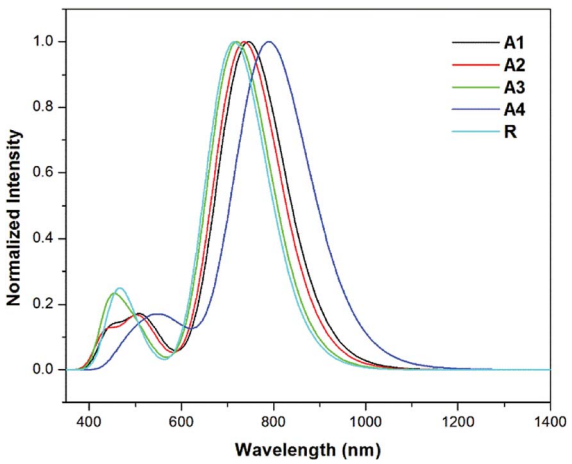

Fig. 7 Simulated absorption spectra of the designed molecules (A1–A4) and reference R in the gas phase at the TD- MPW1PW91/6-31G(d,p) level of theory.

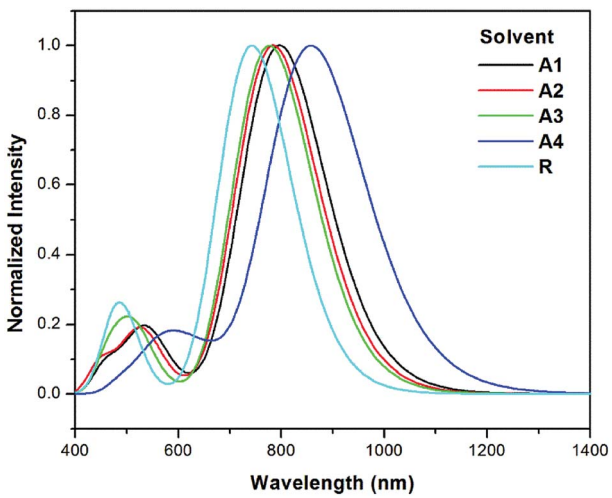

Fig. 8 Simulated absorption spectra of designed molecules (A1–A4) and reference R in solvent (chloroform) at the TD- MPW1PW91/6-31G(d,p) level of theory.

reorganization energies therefore, these two designed molecules have similar electron mobilities. The order of the electron mobility for the designed molecules is **R** < **A1** = **A2** < **A3** < **A4**.

The reorganization energies for the hole of all of the designed molecules are also compared with the reference **R**. The λ_h value of reference compound is 0.0061 eV. The theoretical

Table 4 Reorganization energy and calculated dipole moments of reference R and designed molecules (A1 to A4) at the B3LYP/6-31G(d,p) level of theory

Molecules	λ_e (eV)[a]	λ_h (eV) [b]	μ_g[c]	μ_e[d]	$\mu_e - \mu_g$
R	0.0064	0.0061	0.063	0.176	0.113
A1	0.0063	0.0063	4.725	5.716	0.991
A2	0.0063	0.0062	5.885	6.740	0.855
A3	0.0062	0.0061	6.701	8.489	1.788
A4	0.0048	0.0061	9.282	11.17	1.888

[a] Reorganization energy of the electron. [b] Reorganization energy of the hole. [c] μ_g = Ground state. [d] μ_e = Excited state.

calculated λ_h values for **A1**, **A2**, **A3** and **A4** are 0.0063, 0.0062, 0.0061, and 0.0061 eV as shown in Table 4. **A3** and **A4** have equal λ_h values hence, these two acceptors have the same hole transport mobilities. The order of the hole mobilities of the designed molecules is **R** = **A4** = **A3** < **A2** < **A1**.

6. Dipole moment

Another promising property is the dipole moment of all of the molecules which is calculated at the MPW1PW91/6-31G(d,p) level of theory. The crystallinity of organic solar cells can be enhanced by increasing the solubilities in organic solvents in both the ground and excited states. During fabrication of organic solar cells, the dipole moment is an important parameter. A high value for the dipole moment reveals a good solubility in organic solvents. The calculated dipole moments of reference compound **R** at the ground and excited state are 0.063 and 0.176 debye. The change in the dipole moment between the ground and excited state is 0.113 debye. The dipole moments of **A1**, **A2**, **A3** and **A4** in the gas phase are 4.72, 5.88, 6.70 and 9.28 D, respectively, as shown in Table 4.

All of the designed molecules show a higher dipole moment with respect to the reference compound **R**. Therefore, the solubility of the novel designed molecules should be good in commonly used polar organic solvents (for BHJ organic solar cells such as chloroform and chlorobenzene) as compared to **R**, therefore it would give a reasonably good morphology of film. The changes in the dipole moment of **A1**, **A2**, **A3** and **A4** from the ground to excited state are 5.71, 6.74, 8.84 and 11.17 D, respectively. Among all of the molecules, **A4** has the highest dipole moment which is due to the four electron withdrawing cyano groups which are attached to the end capped acceptor

moiety. The dipole moment of **A3** is higher than **A1** and **A2**. The dipole moment of reference **R** and the designed molecules (**A1–A4**) calculated in a gaseous phase, as well as in solvent, are in order of **A4** > **A3** > **A2** > **A1** > **R**.

In BHJ organic solar cells, molecular fabrication (self-assembly) in film is greatly affected by the dipole moment of the material, as two dipoles arrange themselves in an antiparallel fashion to stimulate self-assembly and improve crystallinity.[55] If the designed molecules have a packing ability then the high value of the dipole moment facilitates the self-assembly of the molecules, and also forms a long chain which provides a strong pathway for the charge mobilities. Therefore, the greater the dipole moment, the higher the charge mobilities. Furthermore, a higher dipole moment facilitates a reduction in the disorder between the donor and the acceptor, which increases the charge mobility between the donor acceptor. Moreover, it also reduces the charge recombination and thereby increases the fill factor (FF).[56] The dipole moment at the ground state as well as in the excited state and their difference are shown in Table 4.

7. Open circuit voltage

The open circuit voltage (V_{oc}) has a vital role in the performance of organic solar cells. It is the maximum amount of current which can be drawn from any optical device. The open circuit voltage is approximately proportional to the difference between the HOMO and LUMO energies of the donor and acceptor molecules, respectively. The LUMO energies of our designed acceptor molecules, including **R**, were aligned with the HOMO of the well-known donor polymer material **PTB7-Th** (E_{HOMO} = −5.20 eV)[57] in Fig. 9, and the HOMO of P3HT IS (E_{HOMO} = −5.12 eV).

The $HOMO_{PTB7\text{-}Th}$–$LUMO_{acceptor}$ energy gap is 1.85, 1.68, 1.79, 1.60, and 1.30 V for **R**, **A1**, **A2**, **A3** and **A4**, respectively. All of the novel designed molecules have comparable V_{oc} with respect to the reference molecule **R** owing to the same difference between the HOMO of donor and the acceptor of the designed molecules. The energy gap of the $HOMO_{donor}$ of P3HT and the $LUMO_{acceptor}$ of the reference and designed molecules (**A1–A4**) are 1.77, 1.60, 1.71, 1.76, and 1.22 V as shown in the ESI.† All of the designed molecules have a comparable V_{oc} value with respect to reference **R**. Among all of the designed molecules, **A2** exhibits a high V_{oc} value. The order of V_{oc} value with both donors (**PTB7-Th** and P3HT) is the same, which is **R** > **A3** > **A2** > **A1** > **A4**.

A low lying LUMO for the acceptor moiety causes higher open circuit voltages and enhances the optoelectronic properties. A low lying LUMO orbital means that the electron can easily be transferred between the donors to the acceptor unit. In addition, the energy gap between the HOMO and LUMO is also important for the transition of electrons between the donors to the acceptor unit and enhances the PCE. Hence, the open circuit voltages are in the order of **A4** < **A1** < **A2** < **A3** < **R**.

8. Transition density matrix and exciton binding energy

The transition density matrixes (TDMs) of the designed molecules, including reference **R**, were computed to estimate the nature of the transition. The MPW1PW91/6-31G(d,p) level of theory was used to derive the absorption and emission of the S_1 state in vacuum. In the present study, the effect of hydrogen atoms is neglected by default owing to their very small contributions in transitions. The transition density matrix enables us to evaluate: (i) the interaction between the donor and acceptor moieties with each other in the excited state; (ii) the electronic excitation; and (iii) the electron hole localization.[58] To study it, we divided our molecules into D (donor core unit), B (combined bridge group), and A (end capped acceptors) parts. It is clear from the TDM diagrams (Fig. 10) that the electron coherence of **R** and **A1–A4** is mainly on the diagonal of the donor and combine bridged and is small on the acceptor end-capped

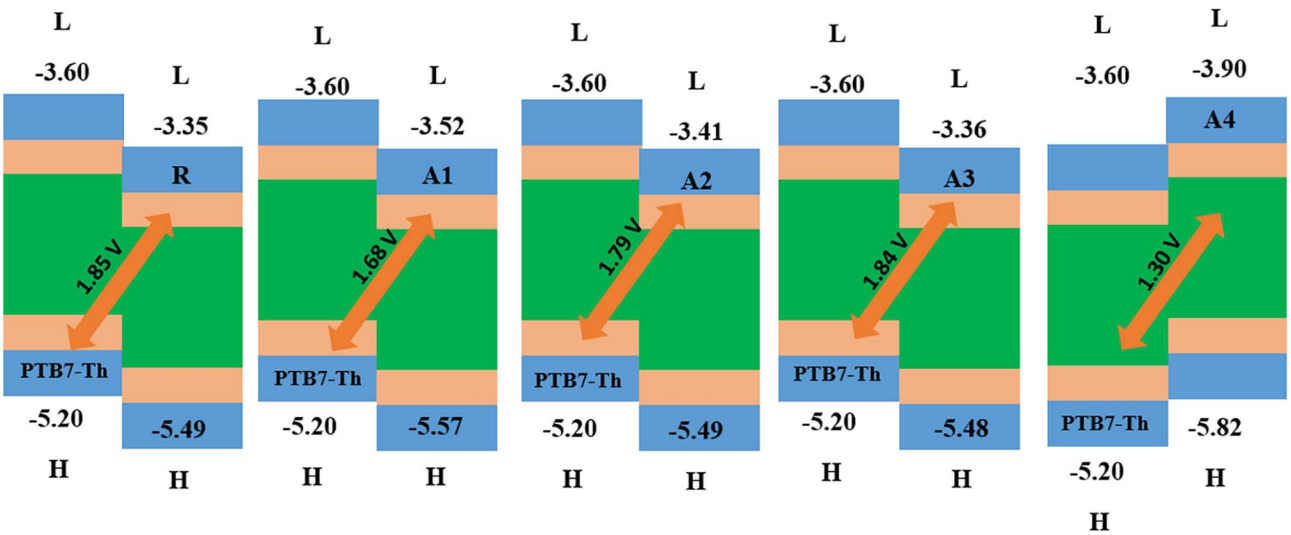

Fig. 9 The V_{oc} of reference R and the designed molecules A1, A2, A3 and A4 with respect to donor material PTB7-Th.

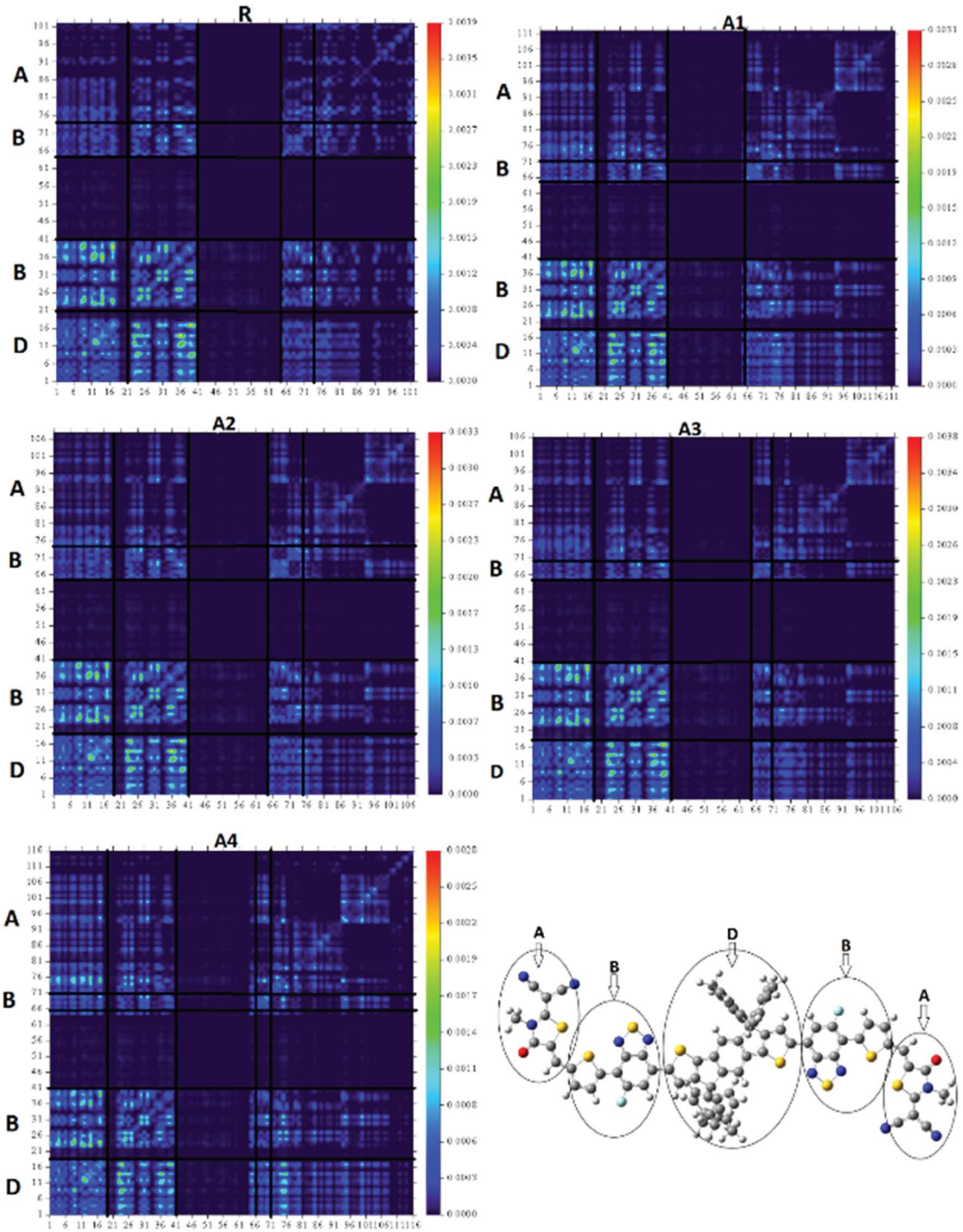

Fig. 10 TDM of reference R and the designed molecules (A1–A4) in the S_1 state.

groups. Additionally, the coefficients of interaction between the donor and acceptor group is in the order of **A4** < **A1** < **A2** < **A3** < **R**. According to this sequence, the coupling of the hole and the electron of **A4** may be lower with respect to the other four molecules, but it could show a higher and easier exciton dissociation in the excited state. The binding energy shows that the **A4** molecule has the largest number of charges and may be easily dissociated into separated charges. Hence, the charge dissociation efficiency of **A4** is higher than that obtained for the other molecules.

The four designed molecules show a higher charge dissociation ability with respect to **R**. This suggests that these molecules can increase the overall current charge density (J_{sc}) in comparison with **R**.

The binding energy is a promising factor in the performance evaluation of organic solar cells and helps the exciton

Table 5 Calculated HOMO–LUMO energy gap E_{H-L}, E_{opt} first singlet excitation energies, and the exciton binding energies (E_b)

Molecules	E_{H-L} (eV)	E_{opt} (eV)	E_b (eV)
R	2.14	1.730	0.41
A1	2.05	1.663	0.387
A2	2.08	1.684	0.396
A3	2.12	1.721	0.399
A4	1.92	1.560	0.360

dissociation potential. The binding energy of all molecules including reference compound **R** was also investigated. The binding energy is a concrete tool for measuring the interaction of the coulombic forces between the hole and the electron, in which a lower value for the binding energy corresponds to a lower coulombic interaction between the electron and the hole, which, in turn, can cause a higher degree of exciton dissociation in the excited state.

The binding energy (E_b) is the difference between the HOMO–LUMO energy gap E_{H-L} and the minimum amount of energy required for the first excitation (E_{opt}). This is the first singlet excited state energy formed from S_0 to S_1 by producing pair of electron and hole.[59–61] E_b can be calculate by using eqn (3).

$$E_b = E_{H-L} - E_{opt} \quad (3)$$

The theoretical binding energies of **R** and **A1–A4** are shown in Table 5

The designed molecules all have a lower binding energy as compared to the reference molecule **R**. In addition, the order of the binding energies for the five molecules is **A4** < **A1** < **A2** < **A3** < **R**, which is in agreement with the TDM result.

9. Charge transfer analysis of acceptor A4 and polymer donor PTB7-Th

To obtain some information about the charge transfer (CT) between **A4** and **PTB7-Th**, the complex was analyzed for CT analysis (Fig. 11). Among all of the molecules, the **A4** molecule

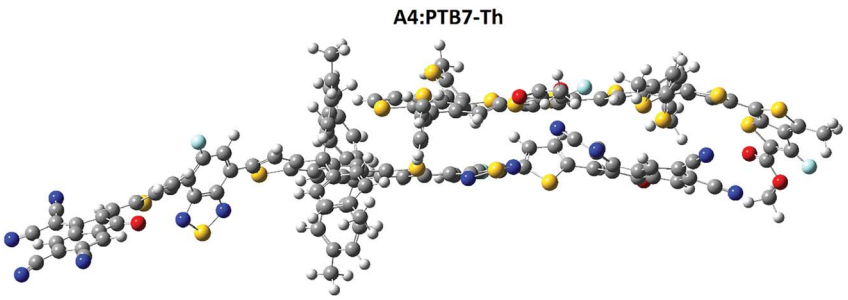

Fig. 11 Charge transfer between **A4** and **PTB7-Th**, the complex geometry was analyzed for charge transfer analysis at the MPW1PW91/6-31G(d,p) level of theory.

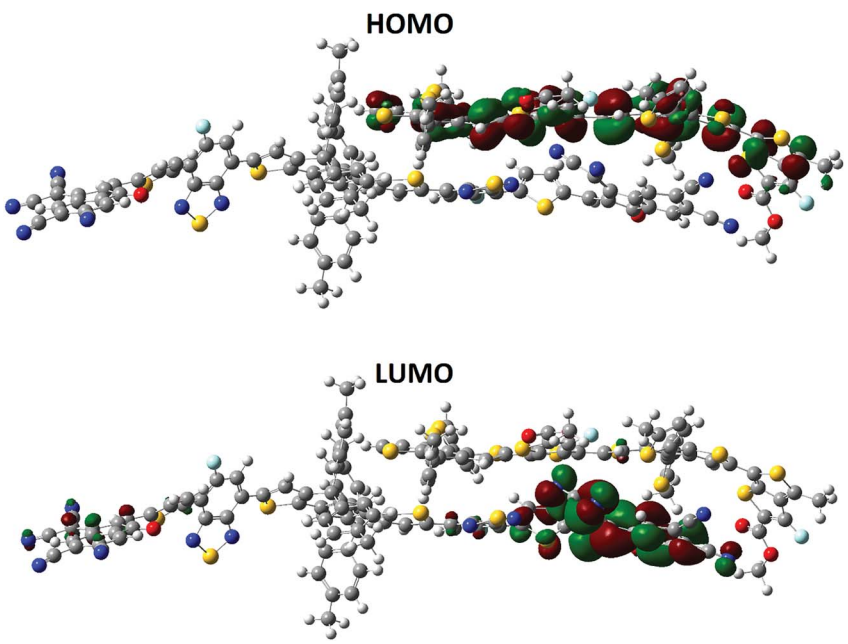

Fig. 12 Distribution patterns of the frontier molecular orbitals (HOMO) and LUMO of **A4** and **PTB7-Th** at the B3LYP/6-311G(d,p) level of theory.

has a low reorganization energy and hence a high electron mobility, therefore the charge transfer between **A4** and **PTB7-Th** was investigated.

The polymer **PTB7-Th** interacts with **A4** in such a way that the polymer is parallel to the combined bridge and end capped acceptor group, which facilitate the charge transfer between the donor and the acceptor unit. The relative orientation of **A4** and **PTB7-Th** has a significant effect on the electronic structure of the complex. The dipole moment of the complex was calculated as the presence of a dipole from **PTB7-Th** in the acceptor has been suggested as a reason for the efficient exciton dissociation at the **A4**/**PTB7-Th** interface.[62–65] The dipole μ in the **A4** : **PTB7-Th** complex is due to electrostatic interactions of the permanent electric moment of **PTB7-Th** with that of **A4**.

Previously published literature reveals that the dipole moment of the complex in governed by the charge transfer. In our case, the orientation of the dipole is in accordance with this statement. The dipole moment vector originates from the polymer side and points towards the end-capped acceptor group of **A4**. The HOMO–LUMO distribution pattern and the electronic structure of the complex were calculated at the MPW1PW91/6-31G(d,p) level of theory. The HOMO density is mainly spread all over the donor polymer **PTB7-Th**, while the LUMO is distributed on the bridge and end-capped acceptor group of **A4**, (Fig. 12). The orbital diagram shows that the HOMO-to-LUMO excitation is a charge transfer from the donor polymer to the acceptor **A4**. The shifting of the density from the donor to the acceptor is concrete evidence for the charge transfer between the different groups.

10. Conclusion

Four novel A–D–A type small molecules (**A1**, **A2**, **A3** and **A4**) were evaluated as acceptors for non-fullerene organic solar cells. These compounds contain indacenodithiophene as a central core unit, monofluoro substituted benzothiadiazole (FBT) as a donor acceptor (DA) combine bridge and different end capped acceptor groups. Various optoelectronic properties of the four molecules were compared with a known reference molecule **R**. The M06-2X. CAM-B3LYP, B3LYP, MPW1PW91, and ωB97XD, with 6-31G(d,p) basis sets were used for the simulation of the UV-Vis spectra of the reference compound **R**. Overall, the designed molecules show better optoelectronic properties as compared to **R**, mainly owing to their electron withdrawing end groups. Molecule **A4** displays a broad absorption in the visible region in the gas phase (λ_{max} = 789.8 nm), as well as in chloroform solvent (λ_{max} = 858.6 nm) and has the lowest HOMO–LUMO band gap (1.92 eV) of all of the five molecules. The lower electron reorganization energy, as compared to the hole reorganization energy, shows that the molecules had superior electron mobilities. The lower values for the electron reorganization energy transfer for **A1–A4** as compared to that of **R** suggest that the novel molecules are suitable for use as acceptors with efficient electron transport in photovoltaic devices. Furthermore, the transition density matrix calculations show a higher charge dissociation ability for **A1–A4** in comparison with that of **R**, which suggests a higher overall current charge density (J_{sc}) for those molecules. The band-gap for exciton formation, as measured by the difference between LUMO energy levels of **A1–A4** and the HOMO level of a molecular model of polymer **PTB7-Th**, range from 1.30 to 1.85 eV. In summary, all four of the A–D–A type small molecules **A1–A4** have better optoelectronic properties as compared to **R** and can therefore be used as organic solar cells.

Conflicts of interest

There are no conflicts to declare.

Acknowledgements

The computations/simulations/SIMILAR were performed on resources provided by the Swedish National Infrastructure for Computing (SNIC) at Umeå University, 901 87, Umeå, Sweden. The authors acknowledge the financial and technical support from the Punjab Bio-energy Institute (PBI) and the University of Agriculture Faisalabad (UAF).

References

1 Y. Li, *Acc. Chem. Res.*, 2012, **45**, 723–733.
2 Y. Lin, Y. Li and X. Zhan, *Chem. Soc. Rev.*, 2012, **41**, 4245–4272.
3 J. Chen and Y. Cao, *Acc. Chem. Res.*, 2009, **42**, 1709–1718.
4 G. Li, R. Zhu and Y. Yang, *Nat. Photonics*, 2012, **6**, 153.
5 L. Lu, T. Zheng, Q. Wu, A. M. Schneider, D. Zhao and L. Yu, *Chem. Rev.*, 2015, **115**, 12666–12731.
6 D. Deng, Y. Zhang, J. Zhang, Z. Wang, L. Zhu, J. Fang, B. Xia, Z. Wang, K. Lu and W. Ma, *Nat. Commun.*, 2016, **7**, 13740.
7 X. Xu, T. Yu, Z. Bi, W. Ma, Y. Li and Q. Peng, *Adv. Mater.*, 2018, **30**, 1703973.
8 G. Zhang, K. Zhang, Q. Yin, X.-F. Jiang, Z. Wang, J. Xin, W. Ma, H. Yan, F. Huang and Y. Cao, *J. Am. Chem. Soc.*, 2017, **139**, 2387–2395.
9 T. Kumari, S. M. Lee, S.-H. Kang, S. Chen and C. Yang, *Energy Environ. Sci.*, 2017, **10**, 258–265.
10 G. Yu, J. Gao, J. C. Hummelen, F. Wudl and A. J. Heeger, *Science*, 1995, **270**, 1789–1791.
11 T. Liu and A. Troisi, *Adv. Mater.*, 2013, **25**, 1038–1041.
12 S. Holliday, R. S. Ashraf, C. B. Nielsen, M. Kirkus, J. A. Röhr, C. H. Tan, E. Collado-Fregoso, A. C. Knall, J. R. Durrant and J. Nelson, *J. Am. Chem. Soc.*, 2015, **137**, 898–904.
13 K. Sivula, C. K. Luscombe, B. C. Thompson and J. M. Fréchet, *J. Am. Chem. Soc.*, 2006, **128**, 13988–13989.
14 Y. Zhang, H.-L. Yip, O. Acton, S. K. Hau, F. Huang and A. K.-Y. Jen, *Chem. Mater.*, 2009, **21**, 2598–2600.
15 Y. Lin and X. Zhan, *Acc. Chem. Res.*, 2015, **49**, 175–183.
16 R. B. Ross, C. M. Cardona, D. M. Guldi, S. G. Sankaranarayanan, M. O. Reese, N. Kopidakis, J. Peet, B. Walker, G. C. Bazan and E. Van Keuren, *Nat. Mater.*, 2009, **8**, 208.
17 C. Yan, S. Barlow, Z. Wang, H. Yan, A. K.-Y. Jen, S. R. Marder and X. Zhan, *Nat. Rev. Mater.*, 2018, **3**, 18003.
18 J. Hou, O. Inganäs, R. H. Friend and F. Gao, *Nat. Mater.*, 2018, **17**, 119.

19 P. Cheng, G. Li, X. Zhan and Y. Yang, *Nat. Photonics*, 2018, **12**, 131.
20 J. Liu, S. Chen, D. Qian, B. Gautam, G. Yang, J. Zhao, J. Bergqvist, F. Zhang, W. Ma and H. Ade, *Nat. Energy*, 2016, **1**, 16089.
21 X. Zhan, Z. a. Tan, B. Domercq, Z. An, X. Zhang, S. Barlow, Y. Li, D. Zhu, B. Kippelen and S. R. Marder, *J. Am. Chem. Soc.*, 2007, **129**, 7246–7247.
22 G. Gao, N. Liang, H. Geng, W. Jiang, H. Fu, J. Feng, J. Hou, X. Feng and Z. Wang, *J. Am. Chem. Soc.*, 2017, **139**, 15914–15920.
23 Y. Lin, J. Wang, Z. G. Zhang, H. Bai, Y. Li, D. Zhu and X. Zhan, *Adv. Mater.*, 2015, **27**, 1170–1174.
24 S. Dai, F. Zhao, Q. Zhang, T.-K. Lau, T. Li, K. Liu, Q. Ling, C. Wang, X. Lu and W. You, *J. Am. Chem. Soc.*, 2017, **139**, 1336–1343.
25 F. Zhao, S. Dai, Y. Wu, Q. Zhang, J. Wang, L. Jiang, Q. Ling, Z. Wei, W. Ma and W. You, *Adv. Mater.*, 2017, **29**, 1700144.
26 Z. Luo, H. Bin, T. Liu, Z. G. Zhang, Y. Yang, C. Zhong, B. Qiu, G. Li, W. Gao and D. Xie, *Adv. Mater.*, 2018, **30**, 1706124.
27 S. Li, L. Ye, W. Zhao, X. Liu, J. Zhu, H. Ade and J. Hou, *Adv. Mater.*, 2017, **29**, 1704051.
28 J. Wang, W. Wang, X. Wang, Y. Wu, Q. Zhang, C. Yan, W. Ma, W. You and X. Zhan, *Adv. Mater.*, 2017, **29**, 1702125.
29 J. Zhu, Z. Ke, Q. Zhang, J. Wang, S. Dai, Y. Wu, Y. Xu, Y. Lin, W. Ma and W. You, *Adv. Mater.*, 2018, **30**, 1704713.
30 T. Li, S. Dai, Z. Ke, L. Yang, J. Wang, C. Yan, W. Ma and X. Zhan, *Adv. Mater.*, 2018, **30**, 1705969.
31 W. Wang, C. Yan, T. K. Lau, J. Wang, K. Liu, Y. Fan, X. Lu and X. Zhan, *Adv. Mater.*, 2017, **29**, 1701308.
32 B. Jia, S. Dai, Z. Ke, C. Yan, W. Ma and X. Zhan, *Chem. Mater.*, 2017, **30**, 239–245.
33 B. Kan, J. Zhang, F. Liu, X. Wan, C. Li, X. Ke, Y. Wang, H. Feng, Y. Zhang and G. Long, *Adv. Mater.*, 2018, **30**, 1704904.
34 S. Li, L. Zhan, F. Liu, J. Ren, M. Shi, C. Z. Li, T. P. Russell and H. Chen, *Adv. Mater.*, 2018, **30**, 1705208.
35 Z. Fei, F. D. Eisner, X. Jiao, M. Azzouzi, J. A. Röhr, Y. Han, M. Shahid, A. S. Chesman, C. D. Easton and C. R. McNeill, *Adv. Mater.*, 2018, **30**, 1705209.
36 W. Zhao, S. Li, H. Yao, S. Zhang, Y. Zhang, B. Yang and J. Hou, *J. Am. Chem. Soc.*, 2017, **139**, 7148–7151.
37 Y. Wu, H. Bai, Z. Wang, P. Cheng, S. Zhu, Y. Wang, W. Ma and X. Zhan, *Energy Environ. Sci.*, 2015, **8**, 3215–3221.
38 S. Holliday, R. S. Ashraf, A. Wadsworth, D. Baran, S. A. Yousaf, C. B. Nielsen, C.-H. Tan, S. D. Dimitrov, Z. Shang and N. Gasparini, *Nat. Commun.*, 2016, **7**, 11585.
39 G. Zhang, G. Yang, H. Yan, J. H. Kim, H. Ade, W. Wu, X. Xu, Y. Duan and Q. Peng, *Adv. Mater.*, 2017, **29**, 1606054.
40 S. Chen, Y. Liu, L. Zhang, P. C. Chow, Z. Wang, G. Zhang, W. Ma and H. Yan, *J. Am. Chem. Soc.*, 2017, **139**, 6298–6301.
41 D. Baran, R. S. Ashraf, D. A. Hanifi, M. Abdelsamie, N. Gasparini, J. A. Röhr, S. Holliday, A. Wadsworth, S. Lockett and M. Neophytou, *Nat. Mater.*, 2017, **16**, 363.
42 S. Holliday, R. S. Ashraf, C. B. Nielsen, M. Kirkus, J. A. Röhr, C.-H. Tan, E. Collado-Fregoso, A.-C. Knall, J. R. Durrant and J. Nelson, *J. Am. Chem. Soc.*, 2015, **137**, 898–904.
43 Y. Ma, M. Zhang, Y. Tang, W. Ma and Q. Zheng, *Chem. Mater.*, 2017, **29**, 9775–9785.
44 Y. Yang, J. Wang, H. Xu, X. Zhan and X. Chen, *ACS Appl. Mater. Interfaces*, 2018, 18984–18992.
45 M. Frisch, G. Trucks, H. Schlegel, G. Scuseria, M. Robb, J. Cheeseman, G. Scalmani, V. Barone, B. Mennucci and G. Petersson, *Gaussian Inc.*, Wallingford, CT, 2009, vol. 27, p. 34.
46 R. D. Dennington, T. A. Keith and J. M. Millam, Gaussian Inc, 2008.
47 J.-D. Chai and M. Head-Gordon, *Phys. Chem. Chem. Phys.*, 2008, **10**, 6615–6620.
48 T. Yanai, D. P. Tew and N. C. Handy, *Chem. Phys. Lett.*, 2004, **393**, 51–57.
49 B. Civalleri, C. M. Zicovich-Wilson, L. Valenzano and P. Ugliengo, *CrystEngComm*, 2008, **10**, 405–410.
50 Y. Zhao and D. G. Truhlar, *Theor. Chem. Acc.*, 2008, **120**, 215–241.
51 C. Adamo and V. Barone, *J. Chem. Phys.*, 1998, **108**, 664–675.
52 M. Cossi, V. Barone, B. Mennucci and J. Tomasi, *Chem. Phys. Lett.*, 1998, **286**, 253–260.
53 J. H. Zhang, Y. Z. Su, J. H. Song and H. Y. Guo, *Comput. Appl. Chem.*, 2003, **4**, 020.
54 M. Ans, J. Iqbal, B. Eliasson and K. Ayub, *Comput. Mater. Sci.*, 2019, **159**, 150–159.
55 C. J. Takacs, Y. Sun, G. C. Welch, L. A. Perez, X. Liu, W. Wen, G. C. Bazan and A. J. Heeger, *J. Am. Chem. Soc.*, 2012, **134**, 16597–16606.
56 J. C. Blakesley and D. Neher, *Phys. Rev. B: Condens. Matter Mater. Phys.*, 2011, **84**, 075210.
57 Y. Liang, Z. Xu, J. Xia, S. T. Tsai, Y. Wu, G. Li, C. Ray and L. Yu, *Adv. Mater.*, 2010, **22**, E135–E138.
58 M. Ans, J. Iqbal, Z. Ahmad, S. Muhammad, R. Hussain, B. Eliasson and K. Ayub, *ChemistrySelect*, 2018, **3**, 12797–12804.
59 M. E. Köse, *J. Phys. Chem. A*, 2012, **116**, 12503–12509.
60 A. Dkhissi, *Synth. Met.*, 2011, **161**, 1441–1443.
61 B. G. Kim, C. G. Zhen, E. J. Jeong, J. Kieffer and J. Kim, *Adv. Funct. Mater.*, 2012, **22**, 1606–1612.
62 V. Arkhipov, P. Heremans and H. Bässler, *Appl. Phys. Lett.*, 2003, **82**, 4605–4607.
63 C. Marchiori and M. Koehler, *Synth. Met.*, 2010, **160**, 643–650.
64 M. Koehler, M. Santos and M. Da Luz, *J. Appl. Phys.*, 2006, **99**, 053702.
65 S. Baranovskii, M. Wiemer, A. Nenashev, F. Jansson and F. Gebhard, *J. Phys. Chem. Lett.*, 2012, **3**, 1214–1221.